How Donor–Bridge–Acceptor Orientation and Chemical Modification Affect the Thermally Activated Delayed Fluorescence Abilities of Boron-Based Emitters

Jeremy M. Kaminski, Tu V. Chu, Christel M. Marian

Suggested Citation:
Kaminski, J., Chu, T. V., & Marian, C. (2025). How Donor–Bridge–Acceptor Orientation and Chemical Modification Affect the Thermally Activated Delayed Fluorescence Abilities of Boron-Based Emitters. ChemPhotoChem, 9(8), Article e202500033. https://doi.org/10.1002/cptc.202500033

ChemPhotoChem

Research Article
doi.org/10.1002/cptc.202500033

Chemistry Europe
European Chemical Societies Publishing

www.chemphotochem.org

How Donor–Bridge–Acceptor Orientation and Chemical Modification Affect the Thermally Activated Delayed Fluorescence Abilities of Boron-Based Emitters

Jeremy M. Kaminski, Tu V. Chu, and Christel M. Marian*

The photophysical properties of a series of thermally activated delayed fluorescence emitters, comprising a nitrogen-based donor, a phenylene bridge and a boron-based acceptor, are investigated using a combination of density functional theory and multi-reference configuration interaction methods. In addition to singlet and triplet charge-transfer (CT) states, an acceptor-localized low-lying triplet state is found in all compounds. The size of the singlet–triplet gap and the energetic order of the CT and locally excited (LE) states can be modulated by regioisomerism (*ortho*- or *para*-linkage) and the chemical modification of the subunits. Spin-vibronic interactions, introduced through a Herzberg–Teller-type approach, are found to accelerate the intersystem crossing process considerably provided that the CT and LE states are close in energy.

1. Introduction

In search for efficient blue thermally activated delayed fluorescence (TADF) emitters, boron-based donor–acceptor systems have gained increasing attention.[1–9] This interest primarily arises due to the strong electron-accepting properties of the sp^2-hybridized, tri-coordinate boron atom and the extended p(B)-π^*(Ar) conjugation in triarylboranes. In combination with suitable donors comprising a tri-coordinate nitrogen atom such as diphenylamine (**DPA**), 9,9-dimethylacridane (**DMAC**) or 9,9-di-phenylacridane (**DPAC**), promising blue-light-emitting TADF compounds were developed, either as *ortho*-appended[10,11] or *para*-appended[12,13] donor–bridge–acceptor systems. These configurations give rise to electronically excited states of through-space charge-transfer (TSCT) and through-bond charge-transfer (TBCT) type, respectively. The acceptors comprised cyclic boryl compounds such as 9-boraanthryl (**BA**) or 10H-phenoxaboryl (**OB**) groups as well as open forms such as dimesitylboryl (**B**). To gain a deeper understanding of the observed trends, the authors performed quantum chemical calculations using Kohn–Sham density functional theory (KS-DFT) and time-dependent DFT (TD-DFT) methods. Herein, they focused mainly on the photophysical properties of the singlet and triplet CT states, S_{CT} and T_{CT}. As we will show, a triplet LE state, $T_{LE(A)}$, is present in all these systems in energetic proximity of the CT states.

Due to spin statistics, singlet and triplet excited states are populated in a ratio of 1:3 in organic light-emitting diodes (OLEDs). TADF emitters harvest the triplet excitons by thermal upconversion of the T_{CT} population to the S_{CT} state, followed by delayed fluorescence. Requirements for efficient upconversion are a sufficiently small singlet–triplet energy gap, ΔE_{ST}, and a reasonable spin–orbit coupling (SOC) strength. The ΔE_{ST} value of CT states is related to the amount of exchange coupling between the donor and acceptor moieties. In face-to-face oriented TSCT systems, the distance between their π-planes can be used to tune the energy of the CT states and their splitting.[14—17] In metal-free TBCT systems, it is typically the torsional angle between the donor and acceptor moieties that steers the ΔE_{ST} value.[18–20] Because intersystem crossing (ISC) and reverse ISC (rISC) between S_{CT} and T_{CT} states of equal electronic structure are orbitally forbidden, spin–vibronic coupling with a nearby LE state is essential for enhancing the $S_{CT} \leftrightsquigarrow T_{CT}$ transitions in TBCT and TSCT complexes.[14,21–26] The enhancement is particularly pronounced if the LE state is of $n\pi^*$-type or if out-of-plane vibrations mix some $n\pi^*$-character into a $\pi\pi^*$-excited state. Even in the absence of doubly occupied nonbonding orbitals, vibronic interactions can lift the orbital selection rules. In triarylborane phosphors, for example, $\sigma(B) \rightarrow \pi^*(B)$ transitions were shown to accelerate the ISC process.[27]

In this work, we investigate the adiabatic energies of the low-lying CT and LE states and their relative energetic order in a series of emitter molecules (**Figure 1**) using a combination of DFT and multi-reference configuration interaction (MRCI) methods.[28] For the most stable conformer of **DPACoOB**, consisting of a **DPAC** donor and an **OB** acceptor connected in *ortho*-position to a methylated phenylene (**1-Me**) bridge, the effect of spin–vibronic coupling on the ISC and rISC rates is explicitly evaluated. To investigate the influence of π-stacking versus C—H $\leftrightarrow \pi$ interactions, we replaced the **DPAC** donor by **DMAC** and **DPA**,

J. M. Kaminski, T. V. Chu, C. M. Marian
Institute of Theoretical and Computational Chemistry
Faculty of Mathematics and Natural Sciences
Heinrich Heine University Düsseldorf
40204 Düsseldorf, Germany
E-mail: Christel.Marian@uni-duesseldorf.de

Supporting information for this article is available on the WWW under https://doi.org/10.1002/cptc.202500033

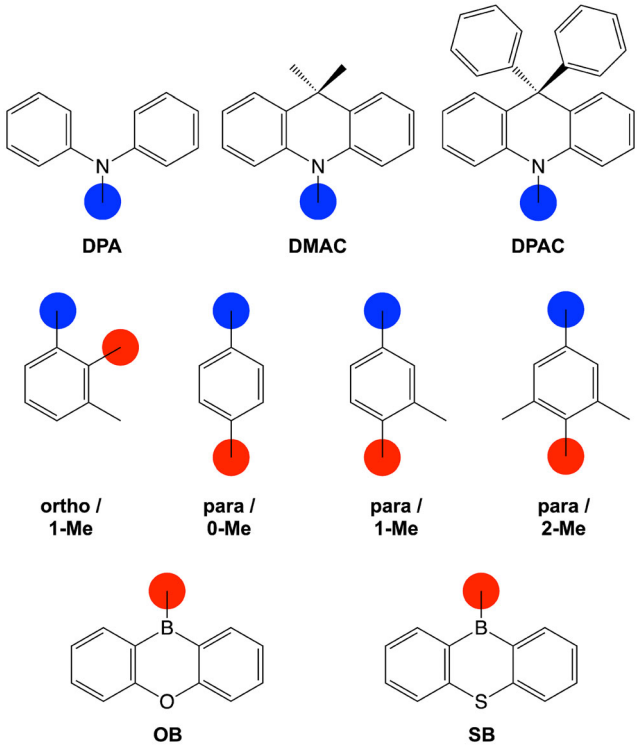

Figure 1. Investigated donor (upper panel), bridge (middle panel), and acceptor (lower panel) moieties. Electron-donating (blue circles) and accepting (red circles) units are cross-linked through a phenylene bridge at the 1,2-positions (*ortho*-regioisomers) or 1,4-positions (*para*-regioisomers).

respectively. By varying the number of methyl groups on the phenylene linker, we systematically study the impact of the steric repulsion between acceptor and linker on the donor–acceptor torsion angle and the photophysical properties of the *para*-appended combination of these substituents. Finally, chemical modification of the acceptor unit is employed to analyze the internal heavy-atom effect on the TADF properties in comparison to the originally used **DPAC** donor and **OB** acceptor.

2. Results and Discussion

2.1. The *Ortho*-Appended DPACoOB Emitter

DPACoOB is one of three molecules in a series studied by Mubarok et al.[11] for which the influence of different acceptor moieties, namely **BA**, **OB,** and **B** on the luminescence was analyzed. These emitters have a rigid backbone due to the *ortho*-connectivity of donor and acceptor. The crystal structure of **DPACoOB** indicates the presence of π–π interactions between one phenyl group of **DPAC** and the **OB** plane. Additionally, a non-bonding electronic interaction between the nitrogen atom of **DPAC** and the boron atom of **OB** may be assumed. Hence, the boron atom is sterically and electronically protected, which improves the chemical and thermal stability of the emitter.[11]

We found two conformers in the electronic ground state. As shown in **Figure 2**, they primarily differ in the orientation of the **DPAC** phenyl groups relative to the acceptor. In **conformer I**, one

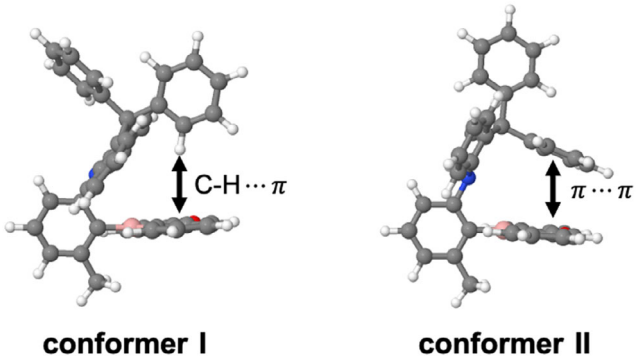

Figure 2. Optimized electronic ground-state conformers of **DPACoOB** at PBE0/def2-SV(P) level of theory in toluene. Conformers **I** and **II** exhibit either C—H···π or π···π interactions, respectively.

of these phenyl groups is perpendicular to the **OB** molecular plane and exerts C—H $\leftrightarrow$ π interactions, similar to the corresponding **DMAC** compound studied in Ref. [10]. **Conformer II** is stabilized by $\pi \leftrightarrow \pi$ interactions between one phenyl residue of the **DPAC** donor and the **OB** acceptor. In agreement with the crystal structure analysis,[11] **conformer II** is preferred over **conformer I** in the electronic ground state. The DFT/MRCI-R2016 calculations place **conformer I** energetically 0.24 eV above **conformer II**. We therefore do not expect **conformer I** to be thermally populated in the electronic ground state.

The experimental absorption spectrum of **DPACoOB** at room temperature in toluene exhibits bands with maxima at 290 and 344 nm and a shoulder at 368 nm.[11] A Gaussian-broadened line spectrum for **conformer II**, calculated at the DFT/MRCI-R2016[28] level of theory, are shown in **Figure 3**. All bands exhibit a systematic hypsochromic shift of 0.10–0.15 eV relative to the experimental spectrum. The lowest-energy absorption band at 356 nm originates from the $S_1 \leftarrow S_0$ excitation, which is mainly a HOMO $\rightarrow$ LUMO transition with donor-to-acceptor CT character. This explains the relatively small oscillator strength ($f = 0.043$) of this transition. The second absorption band with a maximum at 337 nm corresponds to the $S_2 \leftarrow S_0$ excitation, mainly a

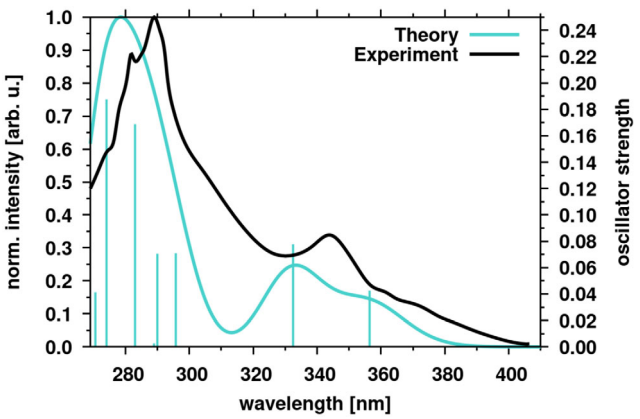

Figure 3. DFT/MRCI-R2016 absorption spectra for **conformer II** (turquoise) of **DPACoOB** in toluene in comparison to experimental results (black).[11] The line spectrum was broadened by Gaussians with 2000 cm full width at half maximum.

HOMO-1 → LUMO transition with LE character localized on the acceptor moiety. The most intense band in the considered wavelength regime arises from several LE transitions, localized either on the donor or acceptor units.

In contrast to the situation in the electronic ground state, the CT states of **conformer I** are located energetically below their counterparts in **conformer II** because the C—H ↔ π interaction stabilizes the negative charge of the **OB** acceptor in the CT states of **conformer I** to a much higher extent than the π-stacking interaction in **conformer II**. To ease the discussion of a possible conformational change in electronically excited **DPACoOB** molecules, all energy levels in **Figure 4** are drawn with respect to a common origin, that is, the ground-state energy of **conformer II**.

The level scheme (Figure 4) reveals significant changes in excitation energies, despite the moderate structural differences between the optimized S_0 and S_{CT}/T_{CT} geometries (Table S3, Supporting Information). In **conformer II**, the bonds connecting nitrogen, boron or oxygen with their direct neighbors differ by at most 0.02 Å in length between the S_0 and S_{CT}/T_{CT} equilibrium structures, leading to minor variations in the corresponding bond angles as well. However, the bite angle between the donor and acceptor moieties, as indicated by the B1–N1 distance, opens up markedly upon optimization of the CT state geometries. Simultaneously, the distance between the π-stacked **DPAC** phenyl residue and **OB** acceptor, reflected in the C41–O1 distance, shrinks. At the ground-state minimum geometry of **conformer II**, the energy difference between the S_{CT} and T_{CT} states is minimal ($\Delta E_{ST,vert} = 0.025$eV), consistent with the value of 0.048 eV calculated by Mubarok et al.[11] at the TDDFT(PBE0)/6-31G** level of theory. Decisive for the TADF properties, however, is the adiabatic value, $\Delta E_{ST,adia}$, or more precisely, the energy splitting $\Delta E_{ST,0-0}$ between the vibrational ground states of these electronic states (see below). Interestingly, the T_{CT} state is not the lowest triplet state at the ground-state geometry according to our calculations. Here, the T_1 state is mainly characterized by a local $\pi\pi^*$ excitation on the acceptor, $T_{LE(A)}$. It is therefore not surprising that the order of states changes when the nuclear arrangement is relaxed in the CT states (Figure 4).

A TheoDORE analysis[29] of the one-particle transition density matrices, performed along a linearly interpolated pathway (LIP) connecting the Franck–Condon (FC) region with the optimized S_{CT} structure (**Figure 5** left), reveals that the electronic structure of the T_1 state changes gradually from a CT contribution of about 10% at the S_0 geometry to about 75% at the S_{CT} minimum geometry. In contrast, the S_1 state largely retains its CT character. Along this relaxation pathway, the S_1 and T_2 potential energy surfaces (PESs) intersect while T_1 and T_2 undergo an avoided crossing. We may therefore expect strong vibronic coupling between these states. A similar picture arises along a LIP connecting the T_{CT} and $T_{LE(A)}$ minima (Figure 5 right). In addition to angular motions of the π-stacked **DPAC** phenyl residue, C—C stretching modes in the **OB** acceptor are excited. The low-frequency vibrational modes promoting the nonadiabatic couplings are torsional and rocking motions of the **OB** acceptor as well as a scissoring mode between the **DPAC** phenyl group and the acceptor moiety.

Difference densities of the S_{CT}, T_{CT}, and $T_{LE(A)}$ states of **conformer II** at their respective minimum geometries are displayed in **Figure 6**. The adiabatic excited-state energies lie all within a narrow range of ≈100 meV. Although the singlet–triplet energy splitting of the CT states ($\Delta E_{ST,adia} = 0.084$ eV, $\Delta E_{ST,0-0} = 0.085$ eV) increases compared to the FC region ($\Delta E_{ST,vert} = 0.025$ eV at the ground-state geometry), it remains small enough to facilitate TADF. Note that the experimental ΔE_{ST} value (0.020 eV), reported by Mubarok et al.[11] was derived from the onsets of the fluorescence and phosphorescence spectra in toluene at 77 K, as the room-temperature fluorescence is substantially red-shifted in this medium. Adiabatically, the T_{CT} and $T_{LE(A)}$ states are almost degenerate according to our calculations.

The fluorescence rate constant of **conformer II** (**Table 1**) matches the expectations for a purely organic donor–acceptor system. Vibronic interactions increase the rate constant only marginally. The radiative lifetime of 185 ns, determined in Herzberg–Teller (HT) approximation, agrees very well with the measured

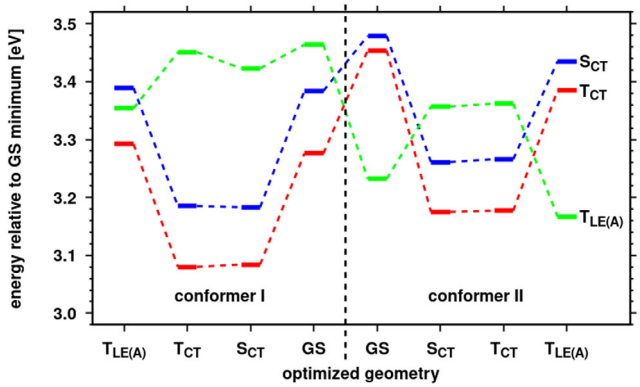

Figure 4. DFT/MRCI-R2016 energy level scheme of **conformer I** and **conformer II** of **DPACoOB** in toluene solution. All adiabatic excitation energies are given relative to the ground-state minimum energy of **conformer II** in eV.

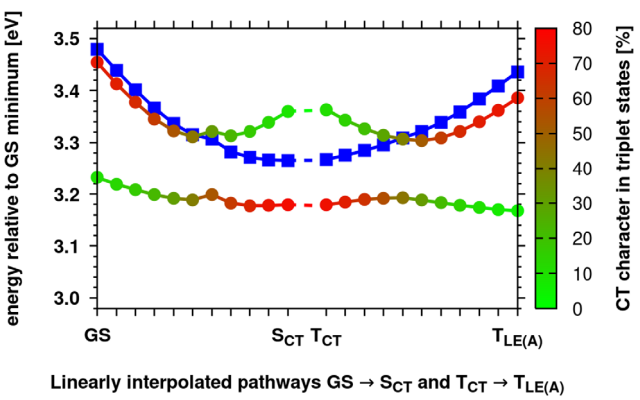

Figure 5. Linearly interpolated pathways between the optimized ground-state (GS) and S, as well as between the optimized T and T geometries (**conformer II**). DFT/MRCI-R2016 vertical energies of the relevant excited singlet (boxes) and triplet (circles) states relative to the ground-state minimum in eV. Along these pathways, the S state can be identified with the S state (blue), whereas the T and T states gradually change their character between T (red) and T (green).

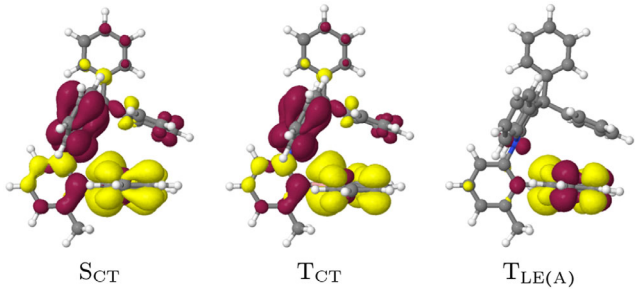

Figure 6. Difference densities (±0.001) of the excited states of **DPACoOB** at their optimized geometries in toluene for **conformer II**. Areas losing electron density in comparison to the S state are shown in red, areas gaining electron density in yellow. Corresponding difference densities for **conformer I** are shown in Figure S2, Supporting Information.

Table 1. FC and FC + HT rate constants (F/ISC/rISC, s^{-1}, 300 K) between low-lying singlet and triplet state of **DPACoOB** for conformers **I** and **II** based on the computed DFT/MRCI energy gaps.

Process	Transition	Conformer I[a)]	Conformer II[a)]	Conformer II[b)]
F	$S_{CT} \rightarrow S_0$	8.7×10^5	5.2×10^6	5.4×10^6
ISC	$S_{CT} \rightsquigarrow T_{CT}$	2.6×10^4	3.8×10^4	3.0×10^6
ISC	$S_{CT} \rightsquigarrow T_{LE(A)}$	8.2×10^3	7.7×10^6	9.6×10^6
rISC	$S_{CT} \rightsquigarrow T_{CT}$	2.2×10^2	4.4×10^2	7.9×10^4
rISC	$S_{CT} \rightsquigarrow T_{LE(A)}$	1.3×10^5	1.3×10^4	7.6×10^4

[a)]FC approach. [b)]FC + HT approach.

prompt fluorescence lifetime of 173.4 ns.[11] While $S_{CT} \rightsquigarrow T_{LE(A)}$ ISC can compete with radiative decay, the nonradiative $S_{CT} \rightsquigarrow T_{CT}$ transition is relatively slow in FC approximation. According to the energy gap law for nested states (weak coupling limit),[30] the rate constant for the latter process is expected to decrease exponentially with increasing ΔE_{ST} value. Indeed, test calculations employing 0–0 energy gaps in a range between 20 and 100 meV confirm these expectations (Figure S3 and Table S6, Supporting Information). In contrast, the $S_{CT} \rightsquigarrow T_{LE(A)}$ transition, which tends toward the strong coupling limit as formulated by Englman and Jortner,[30] appears to be nearly independent of the energy gap. The inclusion of spin-vibronic effects through a HT-like ansatz[31] accelerates the ISC and rISC processes between the CT states by about two orders of magnitude (see Table 1), comparable to the impact of spin–vibronic interactions on the efficient TSCT emitter **TpAT-tFFO**.[14,25,26] At variance with the findings for the FC approximation, the HT rate constants of this ISC process in **DPACoOB** do not obey the energy gap law for nested states. Due to the vibronic coupling between the CT and LE states, the $S_{CT} \rightsquigarrow T_{CT}$ rates seem to inherit the energy dependence from the $S_{CT} \rightsquigarrow T_{LE(A)}$ transition. Varying the 0–0 energy gap in a range between 20 and 100 meV in the VIBES program yields HT ISC rate constants ranging merely between 1×10^6 and $3 \times 10^6\ s^{-1}$ (**Figure 7** and Table S5, Supporting Information). As may be expected, the thermally activated $S_{CT} \rightsquigarrow T_{CT}$ rISC process is much more sensitive with regard to the chosen $\Delta E_{ST,0-0}$ value. The calculated rate constant varies between approximately $2 \times 10^6\ s^{-1}$ for $\Delta E_{ST,0-0} = 20$ meV and

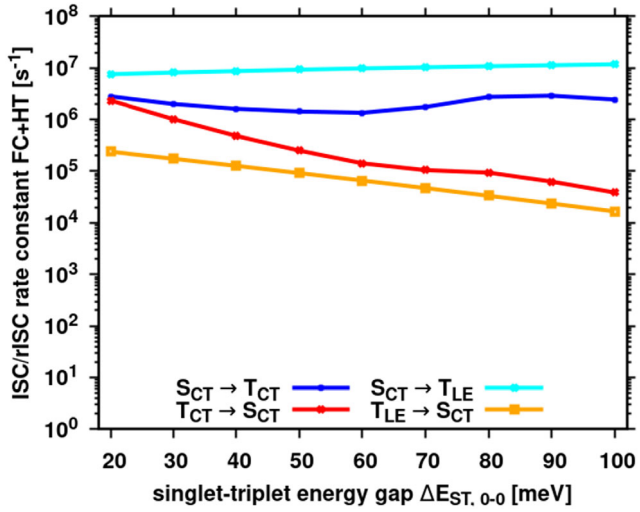

Figure 7. Computed rate constants for ISC and rISC between low-lying singlet and triplet states of **DPACoOB** (**conformer II**) in Herzberg–Teller (HT) approximation at 300 K with varying singlet–triplet energy gap. Note the logarithmic scale of the rate constants.

$4 \times 10^4\ s^{-1}$ for $\Delta E_{ST,0-0} = 100$ meV. Employing the computed 0–0 splitting of 85 meV yields a rate constant of about $10^5\ s^{-1}$ for the backtransfer of triplet excitons in **conformer II** of **DPACoOB** in HT approximation. Spin–vibronic coupling with the nearby $T_{LE(A)}$ state thus provides an explanation for the delayed fluorescence of this conformer inspite of a substantial singlet–triplet splitting.

Component-averaged derivatives of the SOC matrix elements (SOCMEs) with regard to nuclear displacements (Figure S4, Supporting Information) identify an in-plane deformation vibration of the acceptor involving the oxygen atom, normal mode 66 (Figure S5 and S6, Supporting Information), with a harmonic frequency of 665 cm^{-1} as the most prominent promoting mode of the $S_{CT} \leftrightsquigarrow T_{CT}$ ISC and rISC processes. In the acceleration of the $S_{CT} \leftrightsquigarrow T_{LE(A)}$ ISC and rISC processes, C—C stretching modes with harmonic frequencies around 1600 cm^{-1} (Figure S8 and S9, Supporting Information) play prominent roles. Despite larger SOC gradients (Figure S7, Supporting Information) the enhancement of the rISC rate constant by spin-vibronic coupling is smaller than in the $S_{CT} \rightsquigarrow T_{CT}$ upconversion process, presumably due to a lower thermal population of the high-frequency modes.

Fluorescence spectra were calculated for the emissive S_{CT} state at different temperatures in toluene and compared to experimental data[11] (see **Figure 8**). At 77 K, there is good agreement between the calculated ($\lambda_{max} = 409$ nm) and experimental ($\lambda_{max} = 422$ nm) spectra. As may be expected, the computed room-temperature HT spectrum exhibits a moderate bathochromic shift of 1302 cm^{-1} (0.16 eV) due to population of higher vibrational quanta, resulting in a λ_{max} value of 432 nm. Comparison with the corresponding FC spectrum (Figure S12, Supporting Information) shows that the inclusion of vibronic effects does not markedly alter the emission spectrum. The experimental spectrum shows a significantly larger red-shift of 3078 cm^{-1} (0.38 eV) to $\lambda_{max} = 485$ nm. This discrepancy suggests that the observed experimental shift cannot be attributed solely to the

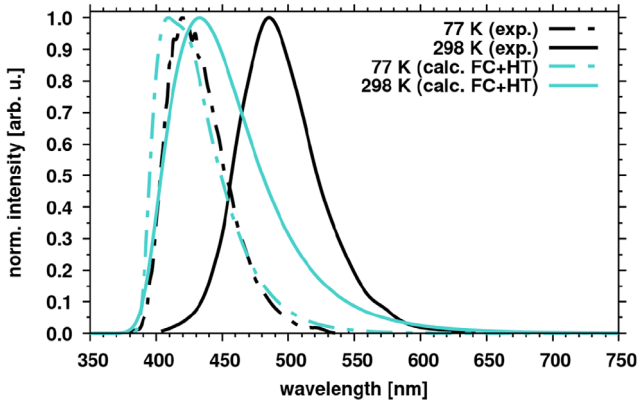

Figure 8. Calculated (turquoise) and experimental (black) emission spectra of **DPACoOB** (**conformer II**) in toluene at 77 K (dashed lines) and 298 K (solid lines). The theoretical spectra were determined in HT approximation.

temperature effect caused by a change in the Boltzmann population of the vibrational levels.

To explore the origin of this effect, we investigated whether the red-shifted emission could stem from **conformer I** as its S_{CT} minimum is energetically favored over the corresponding minimum of **conformer II** (see Figure 4). To populate the S_{CT} state of **conformer I**, an energetically accessible pathway has to be found. The interconversion of the conformer structures does not only require a reorientation of the phenyl group close to the **OB** acceptor. Energetically more demanding is the inversion of the (nonplanar) acredane unit (see Figure S14, Supporting Information). Nudged-elastic band calculations[32,33] indicate barrier heights of ≈0.60 eV on the ground-state PES and of ≈0.40 eV on the S_{CT} PES, which are relatively difficult to overcome (see Figure S13, Supporting Information). We therefore consider the good agreement between the S_{CT} emission spectrum of **conformer I** with the experimental room-temperature spectrum to be accidental.

Analysis of the crystal structure reveals that the donor and acceptor units of two neighboring **DPACoOB** molecules adopt a T-shaped orientation (see Figure S15, Supporting Information). This raised the question whether the red-shifted room-temperature emission in toluene solution could originate from an excimer state. However, preliminary computational results for a dimer did not confirm this hypothesis. Alternatively, solvent reorganization effects could be the cause of the experimentally observed red shift. Although this process is not adequately described by the applied continuum solvent model, there are two experimental indications in favor of this assumption. First, the bathochromic shift of the **DPACoOB** room-temperature emission in the relatively rigid DPEPO film is much smaller than in toluene, which is expected to be solid at 77 K, but exhibits low viscosity at 298 K. Second, a similar dependence of the fluorescence wavelength was observed by Kitamoto et al.[12] for a related *para*-appended compound where conformational effects are unlikely. Notwithstanding the shortcomings of our model in fully recovering the solvent reorganization in liquid toluene, we are confident that our computational approach captures the matrix effects on the dopant in the OLED device very well.

2.2. Chemical Modification of the Donor in *Ortho*-Appended Systems

Donor, bridge, and acceptor units can be systematically modified to fine-tune the photophysical properties of the emitter molecule. First, we investigate the impact of three distinct donor motifs, that is, **DPAC**, **DMAC,** and **DPA** on the adiabatic state ordering when they are cross-linked with the **OB** acceptor in *ortho*-position. **DPAC** and **DMAC** are relatively rigid, whereas **DPA** exhibits higher flexibility. As reported previously, the phenyl groups, attached to the acridane core in **DPAC**, contribute minimally to electronic excitations, but one of them plays a crucial role in nonbonding $\pi \leftrightarrow \pi$ interactions within the molecule (see also Refs. [10,13]). Conversely, **DMAC** features two methyl groups attached to the acridane frame, which facilitate C—H $\leftrightarrow \pi$ interactions. In **DPA**, the rigid tricyclic system is replaced with a more flexible structure. Here, the entire donor participates actively in electronic excitations, and one of its phenyl rings can orient toward the acceptor, enabling π–π stacking, a behavior similar to that observed in **DPAC**.

We do not expect the adiabatic excitation energy of the LE triplet state localized on the acceptor, $T_{LE(A)}$, to be strongly affected by donor modification. However, it is evident from **Figure 9** that an increase of the $\pi \leftrightarrow \pi$ interaction, when going from **DMAC** through **DPA** to **DPAC**, slightly shifts the $T_{LE(A)}$ state to higher energies. In contrast, CT excited states are intrinsically sensitive to the choice of the donor. Like in **conformer I** of **DPACoOB**, C—H $\leftrightarrow \pi$ interaction between one methyl residue of **DMAC** and the negatively charged **OB** acceptor stabilizes the CT states of **DMACoOB**. This stabilization leads to an energetic arrangement of excited states (Figure 9) that enhances the TADF performance, in agreement with the experimentally observed higher ratio of delayed to prompt fluorescence.[10] For **DPA**, the opening of the acridane ring markedly alters the hole distribution on the donor and further lowers the energy of the CT states. Consequently, the $T_{LE(A)}$ state comes to lie energetically higher than the S_{CT} state. This change prevents the $T_{LE(A)}$ state from serving as a mediator in the $S_{CT} \rightsquigarrow T_{CT}$ rISC process. It also becomes apparent that increasing flexibility of the molecule results in a higher ΔE_{ST} value. Compared to **DPAC**, this value

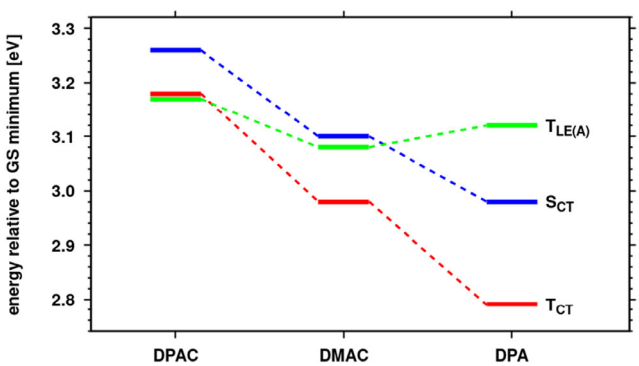

Figure 9. DFT/MRCI-R2016 energy level scheme of **DPACoOB**, **DMACoOB**, and **DPAoOB**. All adiabatic excitation energies are given relative to the ground-state minimum energy of the respective compound in eV.

approximately doubles when **DPA** is chosen as the donor. This result is in line with the conclusion drawn by Wu et al.[34] who set up structure-property relationships for triarylboron-based TADF molecules comprising various donors and dimesitylboryl acceptors.

2.3. Regioisomerism: The *Para*-Appended DPACpOB Emitter

The *para*-linkage of the **DPAC** donor and the **OB** acceptor to the methylphenylene bridge in **DPACpOB** increases the energy gap between the S_{CT} and T_{CT} states substantially in relation to **DPACoOB**. Comparison of the level schemes in **Figure 10** (**1-Me**) and Figure 9 (**DPAC**) reveals that the adiabatic S_{CT} energy is blue-shifted while the adiabatic T_{CT} energy is simultaneously red-shifted in **DPACpOB**, indicating a higher overlap of the hole and particle densities and, consequentially, a stronger donor–acceptor exchange interaction in the *para*-appended emitter. The adiabatic energy of the $T_{LE(A)}$ state varies minimally between the two regioisomers and hence comes to lie in the energy gap between the two CT states in **DPACpOB**. With a rate constant of $k_F = 3.8 \times 10^5\ s^{-1}$ in FC approximation, fluorescence is slowed down by an order of magnitude in comparison to **DPACoOB**, making it more susceptible to competitive nonradiative deactivation processes. $S_{CT} \sim T_{CT}$ ISC proceeds at a rate constant of $k_{ISC} = 8.0 \times 10^5\ s^{-1}$ in FC approximation (see also **Table 2**, 1-**Me**), thus reducing the prompt fluorescence quantum yield. Despite the increased singlet–triplet splitting, the $S_{CT} \sim T_{CT}$ rISC is not substantially slower than in its *ortho*-appended congener. We refrained from carrying out HT-type calculations for **DPACpOB**. However, as the $T_{LE(A)}$ state forms the first excited triplet state at the ground-state geometry and comes to lie adiabatically between S_{CT} and T_{CT} states, we expect spin–vibronic interactions to enhance the rISC rate by one to two orders of magnitude compared to its value of $k_{ISC} = 2.5 \times 10^2\ s^{-1}$ in FC approximation. All in all, we expect this *para*-appended regioisomer to be TADF active, but with lower luminescence quantum yields than the *ortho*-appended regioisomer.

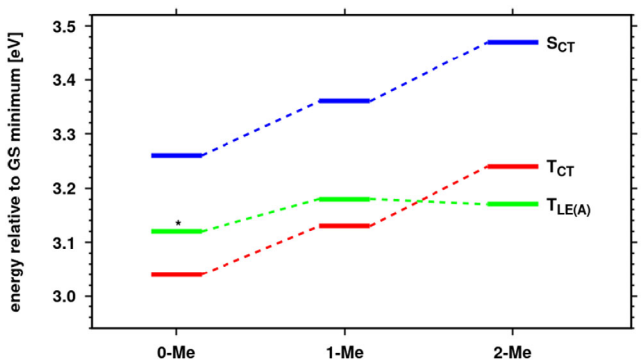

Figure 10. DFT/MRCI-R2016 energy level scheme of **DPACpOB** with modified bridge (**0-Me**, **1-Me**, and **2-Me**). All adiabatic excitation energies are given relative to the ground-state minimum energy of the respective compound in eV. For **0-Me**, the asterisk symbolizes that the $T_{LE(A)}$ state energy was derived from the optimized $S_{LE(A)}$ geometry due to optimization failure.

2.4. Chemical Modification of the Bridge

In other *para*-appended donor–bridge–acceptor systems, the ΔE_{ST} value can easily be manipulated by introducing bulky substituents on the phenylene bridge.[20,35] The question therefore arises whether the twist angle between the donor and acceptor moieties in **DPACpOB** can be changed in a similar way. The closer this angle is to 90°, the smaller ΔE_{ST} values are expected. For **DPACpOB**, we systematically explored the impact of varying numbers of methyl groups, i.e., **0-Me**, **1-Me** and **2-Me**, on the phenyl bridge in *ortho*-position relative to the acceptor. Methyl groups have only minor electronic effects, making them ideal for analyzing conformational changes on the photophysical properties of the *para*-appended emitters.

Increasing the steric hindrance forces the bridge and the acceptor from a twisted conformation with a dihedral angle of 55° (**0-Me**) gradually into an orthogonal arrangement in the electronic ground state of **2-Me**. Simultaneously, the dihedral angle between the donor and the bridge remains nearly orthogonal. Counterintuitively, the addition of methyl groups in *ortho*-position to the acceptor therefore reduces the dihedral angle θ between the donor and acceptor in the electronic ground state, bringing it closer to co-planarity (**0-Me**: 41°, **1-Me**: 15°, **2-Me**: 2°). Similar donor–acceptor twist angles are found for the T_{CT} state (see Table 2), where a change from 28° (**0-Me**) over 13° (**1-Me**) to 3° (**2-Me**) is observed. In the S_{CT} state, the trend is the same. The donor–acceptor twist angles are somewhat larger (**0-Me**: 50°, **1-Me**: 31°, **2-Me**: 21°), but they are far away from 90°.

The adiabatic excitation energy of the $T_{LE(A)}$ state remains nearly constant upon methyl substitution, whereas the S_{CT} and T_{CT} states increase in energy within this series (see Figure 10). Every additional methyl group raises the adiabatic energies of the S_{CT} and T_{CT} by ≈100 meV, despite the fact that the CT character of these states mildly increases, as indicated by the static dipole moments displayed in Table 2. The energy gap between the CT states is kept nearly constant at about 230 meV. While the addition of methyl groups to the linker therefore does not have the desired effect of reducing the ΔE_{ST} value, their impact can be used to position the CT states in the energetic proximity to the $T_{LE(A)}$ state.

The impact of the nuclear arrangement on the electronic structure is most pronounced in the T_{CT} state. Moving from the optimized geometry of the S_{CT} state to the T_{CT} minimum reduces the CT contributions to the T_{CT} wavefunction, thus explaining the substantial lowering of the static electric dipole moment and the increase of the SOCMEs with the S_{CT} wavefunction. For systems in which the LE state lies adiabatically between the CT states, we expect spin-vibronic interactions to improve the TADF abilities. Nevertheless, we consider the *para*-appended boron-based emitters to show inferior TADF performance in comparison to the *ortho*-appended ones.

2.5. Substituting Sulfur for Oxygen

SOC plays a crucial role in the ISC and rISC processes. To exert a heavy-atom effect, we modified the original acceptor

Table 2. Donor–Acceptor twist angle θ (°), electric dipole moments μ (D), adiabatic energy difference ΔE_{adia} (cm^{-1}), component averaged SOCMEs (cm^{-1}) and FC rate constants (s^{-1}, 300 K) for ISC and rISC transitions in *para*-appended **DPAC** and **OB** for varying numbers of methyl substituents on the phenylene bridge.

Bridge	θ	Initial State	Final State	ΔE_{adia}	SOCME	k_{ISC}/k_{rISC}
0-Me	50	S_{CT} ($\mu = 26.18$)	T_{CT} ($\mu = 25.61$)	1759	0.081	2.8×10^4
1-Me	31	S_{CT} ($\mu = 27.97$)	T_{CT} ($\mu = 27.26$)	1909	0.082	8.0×10^5
2-Me	21	S_{CT} ($\mu = 29.44$)	T_{CT} ($\mu = 29.09$)	1826	0.064	5.2×10^4
0-Me	50	S_{CT} ($\mu = 26.18$)	$T_{LE(A)}$ ($\mu = 5.52$)	1094	0.264	4.4×10^5
1-Me	31	S_{CT} ($\mu = 27.97$)	$T_{LE(A)}$ ($\mu = 6.01$)	1504	0.090	4.7×10^3
2-Me	21	S_{CT} ($\mu = 29.44$)	$T_{LE(A)}$ ($\mu = 6.43$)	2403	0.058	2.8×10^5
0-Me	28	T_{CT} ($\mu = 13.88$)	S_{CT} ($\mu = 22.07$)	−1759	0.444	1.5×10^2
1-Me	13	T_{CT} ($\mu = 15.19$)	S_{CT} ($\mu = 23.66$)	−1909	0.386	2.5×10^2
2-Me	3	T_{CT} ($\mu = 16.39$)	S_{CT} ($\mu = 24.70$)	−1826	0.343	2.1×10^2

10H-phenoxaboryl (**OB**) by substituting sulfur for oxygen, resulting in the acceptor unit 10H-phenothiaboryl (**SB**).

Our DFT/MRCI calculations reveal a small singlet–triplet energy gap between the CT states of the *para*-appended compound **DPACpSB** (Table S7, Supporting Information), which is smaller than in **DPACpOB**. Note, however, that the T_{CT} state does not constitute the first excited triplet state in **DPACpSB**. Adiabatically, the $T_{LE(A)}$ state lies more than 0.5 eV below the S_{CT} state, indicating that TADF is not to be expected for this compound. In the corresponding *ortho*-regioisomer, the $S_{LE(A)}$ and $T_{LE(A)}$ states are found at slightly lower energies while the S_{CT} and T_{CT} states are markedly stabilized (Table S7, Supporting Information). This red-shift is not sufficient, however, to bring the $T_{LE(A)}$ state in close energetic proximity to the CT states. On these grounds, we did not investigate the photophysical properties of these sulfur-containing compounds in more detail.

3. Conclusion

In search for suitable blue-light OLED emitters, the class of boron-based TADF emitters has proven to be highly promising. There are many ways to modify the molecular framework of a donor–bridge–acceptor system. In this quantum chemical study, we systematically investigate the influence of the donor–acceptor orientation in *ortho*- and *para*-arrangements on the TADF abilities. Moreover, the donor strength and rigidity is modulated and the impact of an internal heavy-atom effect on the photophysical properties is studied.

Starting with the experimentally verified TADF emitter **DPACoOB**,[11] which consists of a **DPAC** donor and an **OB** acceptor connected in *ortho*-position to a methylated phenylene (**1-Me**) bridge, we found an acceptor-localized excited triplet state, $T_{LE(A)}$, in close energetic proximity to the previously known S_{CT} and T_{CT} states. This $T_{LE(A)}$ state couples vibronically to the T_{CT} state, thus enhancing the upconversion of the triplet population to the fluorescent S_{CT} state. This spin-vibronic mechanism accelerates the rISC by two orders of magnitude brings its rate constant in good agreement with the experimentally determined value.

When the phenyl residues of the acridane donor are replaced by methyl groups, the C—H $\leftrightarrow \pi$ interaction between **DMAC** and the negatively charged **OB** acceptor stabilizes the CT states of **DMACoOB**. This stabilization has a two-fold effect. It leads to a red-shift of the emission and an energetic arrangement of the CT and LE states that is expected to enhance the TADF performance, in agreement with the experimentally observed higher ratio of delayed to prompt fluorescence in comparison to **DPACoOB**.[10,11] The less rigid **DPA** donor further lowers the energy of the CT states and increases the ΔE_{ST} value, thus preventing the $T_{LE(A)}$ state from serving as a mediator in the $S_{CT} \rightsquigarrow T_{CT}$ rISC process.

In the *para*-appended **DPACpOB**, fluorescence is slowed down by an order of magnitude in comparison to the *ortho*-appended **DPACoOB**, making it more susceptible to competitive nonradiative deactivation processes. Although the ΔE_{ST} value is markedly increased in this congener, the rISC rate constants are comparable in both systems. We therefore expect **DPACpOB** to be TADF active, but with lower luminescence quantum yields than the *ortho*-appended regioisomer.

Counterintuitively, the addition of methyl groups in *ortho*-position to the acceptor reduces the dihedral angle between the *para*-appended donor and acceptor units in the electronic ground state of **DPACpOB**, bringing them closer to co-planarity. Therefore, the addition of methyl groups to the linker does not have the desired effect of reducing the ΔE_{ST} value. However, their impact can be used to position the CT states in the energetic proximity to the $T_{LE(A)}$ state.

Introduction of a sulfur atom in the acceptor does not show the expected acceleration of the ISC and rISC processes due to an internal heavy-atom effect because the lowest excited triplet state adopts LE character in **DPACpSB** and **DPACoSB** and is located far below the CT states. We therefore expect these compounds to be nonemissive at room temperature.

Summarizing, chemical modification of the donor, bridge and acceptor in boron-based TADF emitters can be used to tune the energetic position of the CT states with regard to an acceptor-localized T which is an essential mediator for accelerating the rISC process by spin–vibronic interactions.

4. Computational Methods

The electronic ground and excited-state geometries were optimized with Gaussian16[36] using (TD)DFT including the

Tamm–Dancoff approximation (TDA) for excited triplet states. Throughout, the def2-SV(P) atomic orbital basis set[37] was employed in the calculations. Several density functionals were tested in the geometry optimization step of **DPACoOB**. Analysis of the data revealed that dispersion corrections,[38] included either explicitly or through the density functional, lead to too strong intramolecular interactions and underestimate the distance between the phenyl residue of the **DPAC** donor and the **OB** acceptor by up to 0.3 Å. We finally opted for the PBE0[39,40] density functional without dispersion corrections for all structure optimizations as this hybrid functional gave the best overall agreement with the X-ray parameters[11] (Table S2, Supporting Information). Analytic harmonic vibrational frequencies were computed with Gaussian16. Solvation effects (toluene) were considered via the polarizable continuum model[41] (PCM) using the solvent excluding surface (SES) implemented in Gaussian16. Note, that the PCM considers the solvent response to the electronic transition density and does not account for solvent reorganization effects, in contrast to state-specific solvent models based on the difference density. We have refrained from applying a corrected linear response solvent model in the present case because it was found to overshoot drastically in donor–acceptor compounds with highly polar CT excited states.[20]

Molecular orbitals for subsequent excited-state calculations were generated with Turbomole[42] employing the BH-LYP[43,44] density functional. The auxiliary basis sets of Weigend[45] were used for the resolution-of-the-identity approximation of the two-electron integrals. Excitation energies and photophysical properties were calculated with the DFT/MRCI method[46,47] in the R2016 parametrization of the Hamiltonian[28] with the tight configuration selection threshold of 0.8. This method performs much better than TDDFT (Figure S1, Supporting Information) in reproducing the general shape of the absorption spectrum spectrum of **DPACoOB**. Unlike TDDFT conjunction with the PBE0[39,40] hybrid functional or the optimally tuned, long-range corrected LC-HPBE[48] or B97X-D[49] functionals, the DFT/MRCI-R2016 Hamiltonian[28] yields balanced results for the CT and LE transitions (Table S1, Supporting Information). Fragment-based analyses of the DFT/MRCI-R2016 wavefunctions were performed with the TheoDORE tool box.[29]

Radiative rate constants in Franck–Condon (FC) approximation were determined according to the well-known Einstein formula. To check whether vibronic effects accelerate fluorescence, electric dipole transition moments and their numerical derivatives were employed to compute fluorescence rate constants in HT approximation according to

$$k_F^{HT} = \int I^{HT}(\omega)d\omega = \frac{4}{3\hbar c_0^3}\frac{\int \omega^3 S^{HT}(\omega)d\omega}{\int S^{FC}(\omega)d\omega} \tag{1}$$

where $I^{HT}(\omega)$ is the frequency dependent intensity of the computed HT spectrum, $\hbar$ is Planck's constant divided by 2π, c_0 is the vacuum speed of light and $S^{HT}(\omega)$ and $S^{FC}(\omega)$ are the HT and FC spectral densities, respectively, obtained by a fast Fourier transformation of the autocorrelation function in the time domain.[31]

SOCMEs between target singlet and triplet states were calculated with the spin–orbit coupling kit (SPOCK)[50,51] using the Breit–Pauli Hamiltonian in atomic mean-field approximation.[52,53] Derivatives of the SOCMEs with respect to the mass-weighted normal coordinates were determined by two-point finite-difference techniques using a step size of 0.1 units. Rate constants for ISC and rISC in the framework of Fermi's golden rule were determined in FC or HT approximation by means of a Fourier transform approach, as implemented in the VIBES program.[31,35,54] Temperature effects were included by assuming a Boltzmann distribution in the initial electronic state. The time correlation function was multiplied by a Gaussian damping function of 10 cm^{-1} full width at half maximum (FWHM) before numerical integration on a time interval of 3000 fs using 65536 grid points. The sensitivity of the computed rate constants with regard to variations of these technical parameters was found to be marginal (Table S4, Supporting Information). In the FC approximation, the rate constant for the $S_a \rightsquigarrow T_b$ ISC at a given temperature is computed as the sum of squared electronic SOCMEs between the initial singlet state S_a at its minimum geometry and the three triplet sublevels T_b^α, multiplied by the Boltzmann and FC weighted density of vibrational states according to

$$k_{ISC_{ab}}^{FC}(T) = \frac{2\pi}{\hbar Z}\sum_\alpha |\langle \Psi_{T_b^\alpha} | \hat{\mathcal{H}}_{SO} | \Psi_{S_a} \rangle|_{\mathbf{Q}_0}^2 \times \sum_k e^{\frac{-(E_{ak}-E_{a0})}{k_B T}} \sum_j |\langle v_{bj} | v_{ak} \rangle|^2 \, \delta(E_{ak} - E_{bj}) \tag{2}$$

where k_B is the Boltzmann constant and $Z = \sum_k e^{\frac{-(E_{ak}-E_{a0})}{k_B T}}$ the partition function of the initial state. In the HT approximation, the SOC is expanded as a function of the normal coordinates **Q** of the initial state about $\mathbf{Q}_0$ and the expansion is terminated after the linear term yielding[23,31,55]

$$k_{ISC_{ab}}^{FC+HT}(T) = \frac{2\pi}{\hbar Z}\Bigg| \sum_\alpha \sum_k e^{\frac{-(E_{ak}-E_{a0})}{k_B T}} \times \sum_j \langle v_{bj} | \langle \Psi_{T_b^\alpha} | \hat{\mathcal{H}}_{SO} | \Psi_{S_a} \rangle|_{\mathbf{Q}_0} + \sum_A \frac{\partial \langle \Psi_{T_b^\alpha} | \hat{\mathcal{H}}_{SO} | \Psi_{S_a} \rangle}{\partial Q_A}\Bigg|_{\mathbf{Q}_0} Q_A | v_{ak} \rangle \Bigg|^2 \times \delta(E_{ak} - E_{bj}) \tag{3}$$

Squaring this expression yields a pure FC term, a mixed FC/HT term and a HT/HT term. Similar formulas result for the reverse $S_a \rightsquigarrow T_b$ process.

Acknowledgements

This research was funded by the Deutsche Forschungsgemeinschaft (DFG, German Research Foundation)—GRK 2482/396890929.

Open Access funding enabled and organized by Projekt DEAL.

Conflict of Interest

The authors declare no conflict of interest.

Data Availability Statement

The data that support the findings of this study are available in the supplementary material of this article.

Keywords: DFT/MRCI · Herzberg–Teller expansion · regioisomerism · spin–orbit coupling · spin-vibronic interaction

[1] L. Ji, S. Griesbeck, T. B. Marder, *Chem. Sci.* **2017**, *8*, 846.
[2] G. Turkoglu, M. E. Cinar, T. Ozturk, *Molecules* **2017**, *22*, 1522.
[3] S. K. Mellerup, S. Wang, *Trends Chem.* **2019**, *1*, 77.
[4] Z. Huang, S. Wang, R. D. Dewhurst, N. V. Ignatév, M. Finze, H. Braunschweig, *Angew. Chem. Int. Ed.* **2020**, *59*, 8800.
[5] S. S. Kothavale, J. Y. Lee, *Adv. Opt. Mater.* **2020**, *8*, 2000922.
[6] H. Lee, D. Karthik, R. Lampande, J. H. Ryu, J. H. Kwon, *Front. Chem.* **2020**, *8*, 373.
[7] H. J. Kim, T. Yasuda, *Adv. Opt. Mater.* **2022**, *10*, 2201714.
[8] J.-Y. Yoo, S. W. Kang, T. H. Ha, C. W. Lee, *J. Mater. Chem. C* **2024**, *12*, 14045.
[9] J. Park, S. Han, U. Jo, S. C. Kim, D. R. Lee, H. J. Ahn, J. Y. Kim, J.-H. Baek, J. Y. Lee, *Mater. Today* **2024**, *75*, 27.
[10] J. Kim, T. Lee, J. Y. Ryu, Y. H. Lee, J. Lee, J. Jung, M. H. Lee, *Organometallics* **2020**, *39*, 2235.
[11] H. Mubarok, W. Lee, T. Lee, J. Jung, S. Yoo, M. H. Lee, *Front. Chem.* **2020**, *8*, 538.
[12] Y. Kitamoto, T. Namikawa, D. Ikemizu, Y. Miyata, T. Suzuki, H. Kita, T. Sato, S. Oi, *J. Mater. Chem. C* **2015**, *3*, 9122.
[13] Y. H. Lee, D. Lee, T. Lee, J. Lee, J. Jung, S. Yoo, M. H. Lee, *Dyes Pigm.* **2021**, *188*, 109224.
[14] Y. Wada, H. Nakagawa, S. Matsumoto, Y. Wakisaka, H. Kaji, *Nat. Photonics* **2020**, *14*, 643.
[15] S. Kumar, L. G. Franca, K. Stavrou, E. Crovini, D. B. Cordes, A. M. Z. Slawin, A. P. Monkman, E. Zysman-Colman, *J. Phys. Chem. Lett.* **2021**, *12*, 2820.
[16] Q. Li, J. Hu, J. Lv, X. Wang, S. Shao, L. Wang, X. Jing, F. Wang, *Angew. Chem. Int. Ed.* **2020**, *59*, 20174.
[17] Y. Song, M. Tian, R. Yu, L. He, *ACS Appl. Mater. Interfaces* **2021**, *13*, 60269.
[18] R. Dhali, D. A. P. Huu, F. Bertocchi, C. Sissa, F. Terenziani, A. Painelli, *Phys. Chem. Chem. Phys.* **2021**, *23*, 378.
[19] F. Di Maiolo, D. K. A. Phan Huu, D. Giavazzi, A. Landi, O. Racchi, A. Painelli, *Chem. Sci.* **2024**, *15*, 5434.
[20] J. M. Kaminski, T. Böhmer, C. M. Marian, *J. Phys. Chem. C* **2024**, *128*, 13711.
[21] M. K. Etherington, J. Gibson, H. F. Higginbotham, T. J. Penfold, A. P. Monkman, *Nat. Comm.* **2016**, *7*, 13680.
[22] R. S. Nobuyasu, Z. Ren, G. C. Griffiths, A. S. Batsanov, S. Data, P. Yan, A. P. Monkman, M. R. Bryce, F. B. Dias, *Adv. Opt. Mater.* **2016**, *4*, 597.
[23] T. J. Penfold, E. Gindensperger, C. Daniel, C. M. Marian, *Chem. Rev.* **2018**, *118*, 6975.
[24] C. M. Marian, *Annu. Rev. Phys. Chem.* **2021**, *72*, 617.
[25] J. M. Kaminski, A. Rodrguez-Serrano, F. Dinkelbach, H. Miranda-Salinas, A. P. Monkman, C. M. Marian, *Chem. Sci.* **2022**, *13*, 7057.
[26] H. Miranda-Salinas, A. Rodriguez-Serrano, J. M. Kaminski, F. Dinkelbach, N. Hiromichi, Y. Kusakabe, H. Kaji, C. M. Marian, A. P. Monkman, *J. Phys. Chem. C* **2023**, *127*, 8607.
[27] Z. Wu, J. Nitsch, J. Schuster, A. Friedrich, K. Edkins, M. Loebnitz, F. Dinkelbach, V. Stepanenko, F. Würthner, C. M. Marian, L. Ji, T. B. Marder, *Angew. Chem. Intl. Ed.* **2020**, *59*, 17137.
[28] I. Lyskov, M. Kleinschmidt, C. M. Marian, *J. Chem. Phys.* **2016**, *144*, 034104.
[29] F. Plasser, *J. Chem. Phys.* **2020**, *152*, 084108.
[30] R. Englman, J. Jortner, *Mol. Phys.* **1970**, *18*, 145.
[31] M. Etinski, V. Rai-Constapel, C. M. Marian, *J. Chem. Phys.* **2014**, *140*, 114104.
[32] V. Ásgeirsson, B. O. Birgisson, R. Bjornsson, U. Becker, F. Neese, C. Riplinger, H. Jónsson, *J. Chem. Theory Comput.* **2021**, *17*, 4929.
[33] F. Neese, *WIREs Comput. Mol. Sci.* **2022**, *12*, e1606.
[34] Z. Wu, F. Li, Y. Zhou, J. Fan, L. Lin, *Mater. Sci. Eng. B-Adv.* **2021**, *270*, 115203.
[35] T. Böhmer, M. Kleinschmidt, C. M. Marian, *J. Chem. Phys.* **2024**, *161*, 094114.
[36] Gaussian 16, Revision A.03, M. J. Frisch, G. W. Trucks, H. B. Schlegel, G. E. Scuseria, M. A. Robb, J. R. Cheeseman, G. Scalmani, V. Barone, G. A. Petersson, H. Nakatsuji, X. Li, M. Caricato, A. V. Marenich, J. Bloino, B. G. Janesko, R. Gomperts, B. Mennucci, H. P. Hratchian, J. V. Ortiz, A. F. Izmaylov, J. L. Sonnenberg, D. Williams-Young, F. Ding, F. Lipparini, F. Egidi, J. Goings, B. Peng, A. Petrone T. Henderson D. Ranasinghe, V. G. Zakrzewski, et al., Gaussian, Inc., Wallingford CT **2016**.
[37] F. Weigend, R. Ahlrichs, *Phys. Chem. Chem. Phys.* **2005**, *7*, 3297.
[38] S. Grimme, S. Ehrlich, L. Goerigk, *J. Comp. Chem.* **2011**, *32*, 1456.
[39] J. P. Perdew, K. Burke, M. Ernzerhof, *Phys. Rev. Lett.* **1996**, *77*, 3865.
[40] C. Adamo, V. Barone, *J. Chem. Phys.* **1999**, *110*, 6158.
[41] J. Tomasi, B. Mennucci, R. Cammi, *Chem. Rev.* **2005**, *105*, 2999.
[42] TURBOMOLE *V7.5* 2020, *a development of University of Karlsruhe and Forschungszentrum Karlsruhe GmbH, 1989-2007, TURBOMOLE GmbH, since 2007; available from* http://www.turbomole.com.
[43] A. D. Becke, *J. Chem. Phys.* **1993**, *98*, 1372.
[44] C. Lee, W. Yang, R. G. Parr, *Phys. Rev. B* **1988**, *37*, 785.
[45] F. Weigend, *Phys. Chem. Chem. Phys.* **2006**, *8*, 1057.
[46] S. Grimme, M. Waletzke, *J. Chem. Phys.* **1999**, *111*, 5645.
[47] C. M. Marian, A. Heil, M. Kleinschmidt, *WIREs Comput. Mol. Sci.* **2019**, *9*, e1394.
[48] O. A. Vydrov, G. E. Scuseria, *J. Chem. Phys.* **2006**, *125*, 234109.
[49] J.-D. Chai, M. Head-Gordon, *Phys. Chem. Chem. Phys.* **2008**, *10*, 6615.
[50] M. Kleinschmidt, J. Tatchen, C. M. Marian, *J. Comput. Chem.* **2002**, *23*, 824.
[51] M. Kleinschmidt, C. M. Marian, *Chem. Phys.* **2005**, *311*, 71.
[52] B. A. Heß, C. M. Marian, U. Wahlgren, O. Gropen, *Chem. Phys. Lett.* **1996**, *251*, 365.
[53] B. Schimmelpfennig, *Atomic Mean-Field Integral (AMFI) Program*, University of Stockholm **1996**.
[54] M. Etinski, J. Tatchen, C. M. Marian, *J. Chem. Phys.* **2011**, *134*, 154105.
[55] J. Tatchen, N. Gilka, C. M. Marian, *Phys. Chem. Chem. Phys.* **2007**, *9*, 5209.

Manuscript received: January 31, 2025
Revised manuscript received: April 28, 2025
Version of record online: June 17, 2025